DOI: 10.24352/UB.OVGU-2017-048 TECHNISCHE MECHANIK, 37, 1, (2017), 28 – 36
submitted: February 13, 2017

Estimation of the Compression Modulus of a Technical Rubber via Cyclic Volumetric Compression Tests

O. Gehrmann, N. H. Kröger, P. Erren, D. Juhre

In many applications for finite element (FE) simulations rubber materials are assumed to be nearly incompressible by applying a high ratio between compression modulus and shear modulus. The compression modulus is commonly given as a constant value in FE analysis. In reality this assumption is not fully correct. Influencing factors like the compressibility of the included filler can lead to a notably change of the compression modulus during mechanical loading. The focus of this work is on the estimation of the cyclic evolution of the compression modulus for a technical ethylene propylene diene rubber (EPDM) by using cyclic volumetric compression tests.

1 Introduction

Although, in most material modeling approaches, rubber is said to be incompressible, many rubber compounds are at least slightly compressible. Zimmermann and Stommel (2013) showed that the FE analysis results of hydrostatic loads superimposed with non-hydrostatic loads can significantly vary with a moderate change of the compression modulus. In recent papers, new modeling approaches for the compression modulus are suggested by e.g. (Horgan and Murphy, 2009a,b,c). The underlying material is assumed to be ideal hyperelastic and the validation with experimental data is based on investigations of Rivlin and Saunders (1951). Further experiments regarding the characterization of the compressive behavior of fluoroelastomers (FKM) and hydrogenated nitrile butadiene rubber (HNBR) are documented in Ilseng et al. (2015). In Rajagopal and Saccomandi (2009) and references within, the modulus of shear is given as a function of the hydrostatic pressure, considering the framework of small deformations. Important and well known effects like material softening and inelastic behavior for cyclic loading in case of rubber materials are not investigated in the cited literature. In this work the cyclic behavior of a technical EPDM in volumetric compression is investigated. The insights shall be applied for future modeling approaches of the compression modulus in FE simulations.

2 Specimen Production and Test Setup

The volumetric compression test is conducted on a MTS 831 Elastomer Test System. The test specimen is a cylinder of EPDM rubber with a diameter of 7.4 mm and a height of approximately 9.9 mm. The test setup is shown in figure 1. The arrow symbolizes the motion of the stamp.

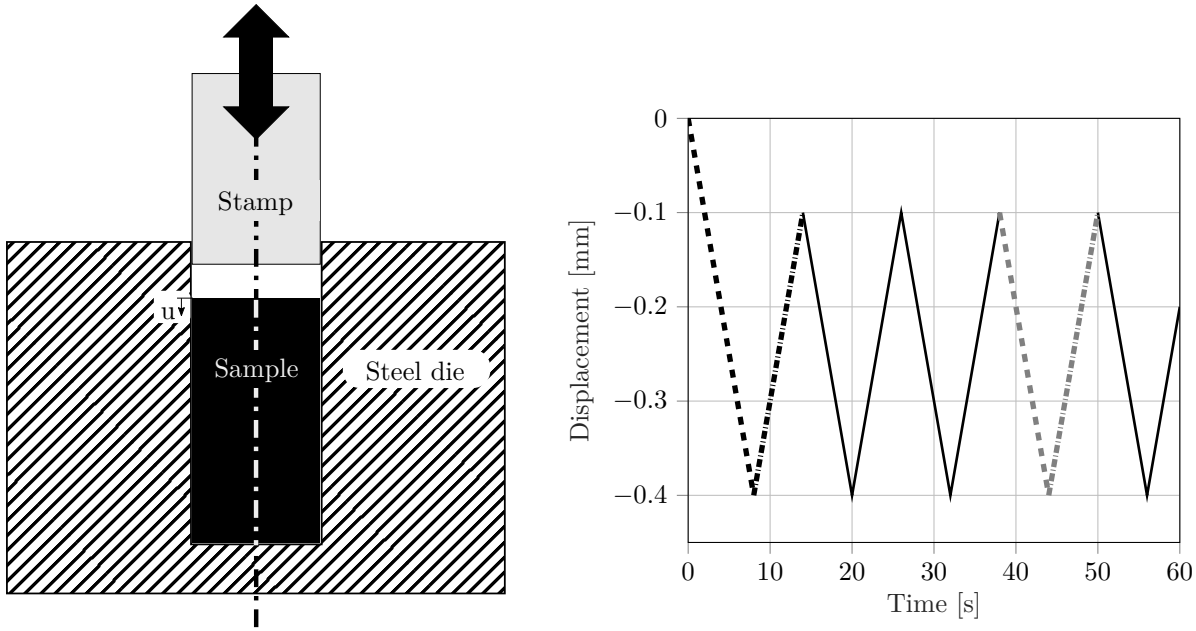

Figure 1: Scheme of the test setup (left) and applied deformation (right; 1^{st} cycle in black dashed, 4^{th} cycle in gray dashed, cf. figure 9).

The EPDM mixture, see table 1, is prepared on a 1.5 liter mixer and admixed with the crosslinking agent and catalysts at the roller. The samples are vulcanized at 160 ℃ for 19 min. Due to shrinkage of the rubber several specimens with varying diameter are molded. The specimens with the tightest fit are chosen. The experiment is displacement driven with a velocity of 0.05 mm/s , see figure 1 (right). The repeated cyclic loading is realized between 0.1 mm and 0.4 mm.

Ingredients	Keltan 4450	Carbon black N-347	Oil sunpar 2280	Zinc oxid	Stearic acid	Sulphur	TBBS	TBzTD
Phr	100	50	40	4	2	0.7	1	3.5

Table 1: Recipe of the investigated EPDM mixture

3 Analytic Example of a Compressed Cylinder

At first view, the applied test procedure (see figure 1) is not applicable to provide any statements about the material behavior of rubber under hydrostatic loadings. The deformation is not fully hydrostatic (see figure 2). However, it can be shown, that the globally measured reaction force is mainly a cause of the hydrostatic fraction of the specimen's total deformation.

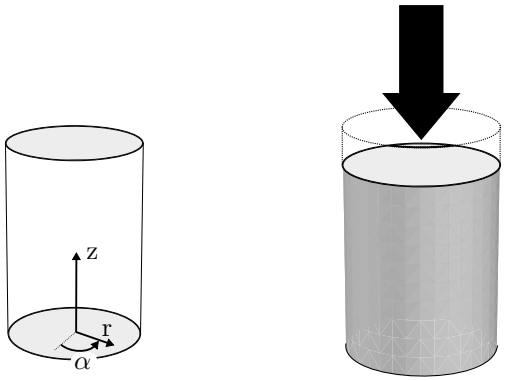

Figure 2: Cylindrical coordinates and exaggerated deformation of the cylindrical specimen during the test.

The displacement vector in cylindrical coordinates is given by

$$u = (u_r, u_\alpha, u_z). \tag{1}$$

For the compression test, shown in figure 1, the assumption of small deformations is reasonable. For a cylinder with rotational symmetry the strain components can be written as e.g. shown by Zienkiewicz et al. (2013)

$$\begin{aligned} \varepsilon_{rr} &= \frac{\partial u_r}{\partial r}, & \varepsilon_{\alpha\alpha} &= \frac{u_r}{r}, & \varepsilon_{zz} &= \frac{\partial u_z}{\partial z}, \\ \varepsilon_{zr} &= \frac{1}{2}\left(\frac{\partial u_r}{\partial r} + \frac{\partial u_z}{\partial z}\right), & \varepsilon_{r\alpha} &= 0, & \varepsilon_{\alpha z} &= 0. \end{aligned} \tag{2}$$

For the demonstration a linear elastic material is assumed. In this case, the stress components in cylindrical coordinates are defined as

$$\begin{aligned} \sigma_{rr} &= \frac{(1-\nu)E}{(1+\nu)(1-2\nu)}\left(\varepsilon_{rr} + \frac{\nu}{1-\nu}(\varepsilon_{\alpha\alpha} + \varepsilon_{zz})\right), \\ \sigma_{\alpha\alpha} &= \frac{(1-\nu)E}{(1+\nu)(1-2\nu)}\left(\varepsilon_{\alpha\alpha} + \frac{\nu}{1-\nu}(\varepsilon_{rr} + \varepsilon_{zz})\right), \\ \sigma_{zz} &= \frac{(1-\nu)E}{(1+\nu)(1-2\nu)}\left(\varepsilon_{zz} + \frac{\nu}{1-\nu}(\varepsilon_{rr} + \varepsilon_{\alpha\alpha})\right), \\ \sigma_{zr} &= \frac{E}{(1+\nu)}\varepsilon_{zr}, \end{aligned} \tag{3}$$

with ν as the Poisson's ratio and E as the Young's modulus. The boundary condition in radial direction is given as a hindered deformation $u_r = 0$. A deformation can only take place in z-direction. By applying the equation

$$K = \frac{E}{3(1-2\nu)} \tag{4}$$

one obtains for the stress components written in matrix shape

$$\boldsymbol{\sigma} = \begin{bmatrix} \frac{3K\nu\varepsilon_{zz}}{(1+\nu)} & 0 & 0 \\ 0 & \frac{3K\nu\varepsilon_{zz}}{(1+\nu)} & 0 \\ 0 & 0 & \frac{3K(1-\nu)\varepsilon_{zz}}{(1+\nu)} \end{bmatrix}, \tag{5}$$

with K as the compression modulus. The decomposition into a non-hydrostatic and a hydrostatic part, yields

$$\boldsymbol{\sigma} = K\varepsilon_{zz}\begin{bmatrix} \frac{3\nu}{(1+\nu)} - 1 & 0 & 0 \\ 0 & \frac{3\nu}{(1+\nu)} - 1 & 0 \\ 0 & 0 & \frac{3(1-\nu)}{(1+\nu)} - 1 \end{bmatrix} + K\varepsilon_{zz}\begin{bmatrix} 1 & 0 & 0 \\ 0 & 1 & 0 \\ 0 & 0 & 1 \end{bmatrix}. \tag{6}$$

Exemplarily, values of 1000 MPa for the compression modulus and of 3 MPa for the Young's modulus are assumed. This yields a Poisson's ratio of $\nu = 0.4995$ after converting equation (4). The application of this value on equation (6) shows that the globally measured behavior can almost be completely referred to the hydrostatic stress response since the non-hydrostatic part is negligible (see equation (7))

$$\boldsymbol{\sigma} = K\varepsilon_{zz}\begin{bmatrix} -6.67\cdot 10^{-4} & 0 & 0 \\ 0 & -6.67\cdot 10^{-4} & 0 \\ 0 & 0 & 1.33\cdot 10^{-3} \end{bmatrix} + K\varepsilon_{zz}\begin{bmatrix} 1 & 0 & 0 \\ 0 & 1 & 0 \\ 0 & 0 & 1 \end{bmatrix}. \tag{7}$$

4 Numerical Simulation of the Compressed Cylinder

A numerical simulation of the compression test is performed. For the simulation, a two-dimensional axisymmetric FE model is used. Accompanied with the creation of the FE model a mesh study is conducted. Four different element sizes are investigated (rough ($NE_{radial} = 6 \times NE_z = 17$), normal ($10 \times 27$), fine ($19 \times 50$), finer ($37 \times 99$)). No significant influence on the results from figure 5 is observable. To obtain an appropriate resolution of the depictions from figure 6, the normal element size is chosen. The FE model for the compressive deformation with the normal element size is schematically shown in figure 3. The symmetry line is symbolized by the dot-dash line and the contact lines are symbolized by the dashed lines. A gap of 5 μm is given between the rubber specimen and the outer contact line.

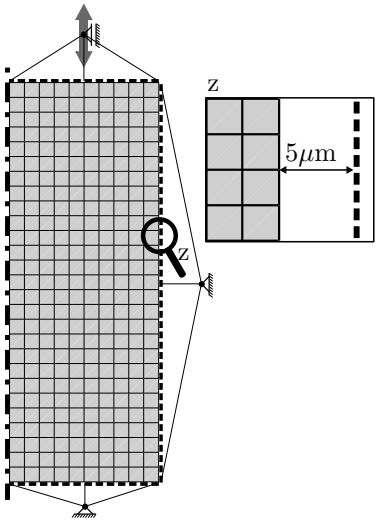

Figure 3: Sketch of the FE model for the compressive deformation with dashed lines as contact lines.

Two different material models are compared. First, the material models are compared under uniaxial tension (see figure 4). Two loading cycles are simulated. The Neo-Hooke material model has a pure hyperelastic behavior since the loading path equals to the unloading path (see Treloar (1944)). The MORPH (Model of Rubber Phenomenology) is able to describe (next to the non-linear behavior) material softening, permanent set and the hysteresis loop of a filled rubber material under large deformations (Besdo and Ihlemann, 2003; Juhre et al., 2011). In both models the hydrostatic part of the stresses are treated identically.

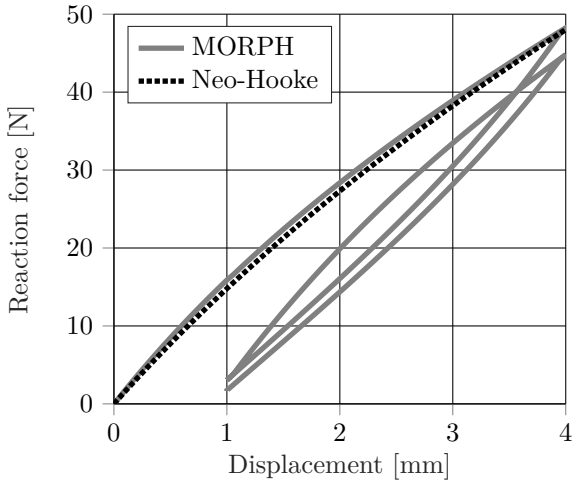

Figure 4: Comparison of the hyperelastic Neo-Hooke material model with the MORPH model by using the global reaction force over the global uniaxial deformation of the specimen.

In case of simulating the compression test from figure 1, no significant difference between these material models is visible (see figure 5). A hysteresis loop or a softening cannot be observed for the MORPH model under these hydrostatic loadings. For both models a constant compression modulus of 2000 MPa is applied. The gap of 5 μm between the rubber specimen and the outer contact line (see figure 3) creates a plateau at the beginning of the global deformation. A similar behavior can be observed in the experimental data and is the motivation for that gap in the FE model.

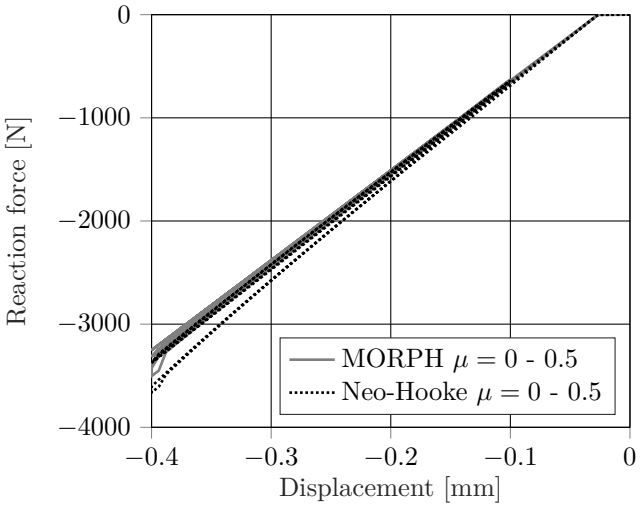

Figure 5: Comparison of the hyperelastic Neo-Hooke material model with the MORPH material model at the compression test.

An indicator is created to measure the level of hydrostatic state within the specimen. The indicator is defined as

$$Indicator_{Hydro} = \frac{\sigma_1 + \sigma_2 + \sigma_3}{3\sigma_1}, \tag{8}$$

with σ_i $(i = 1, 2, 3)$ as the principal Cauchy stresses. The indicator equals to 1.0 for a pure hydrostatic load. Figure 6 shows the specimen exposed to the maximum global deformation of 0.4 mm and with a varied friction coefficient. The numerical values are mapped on the undeformed FE mesh.

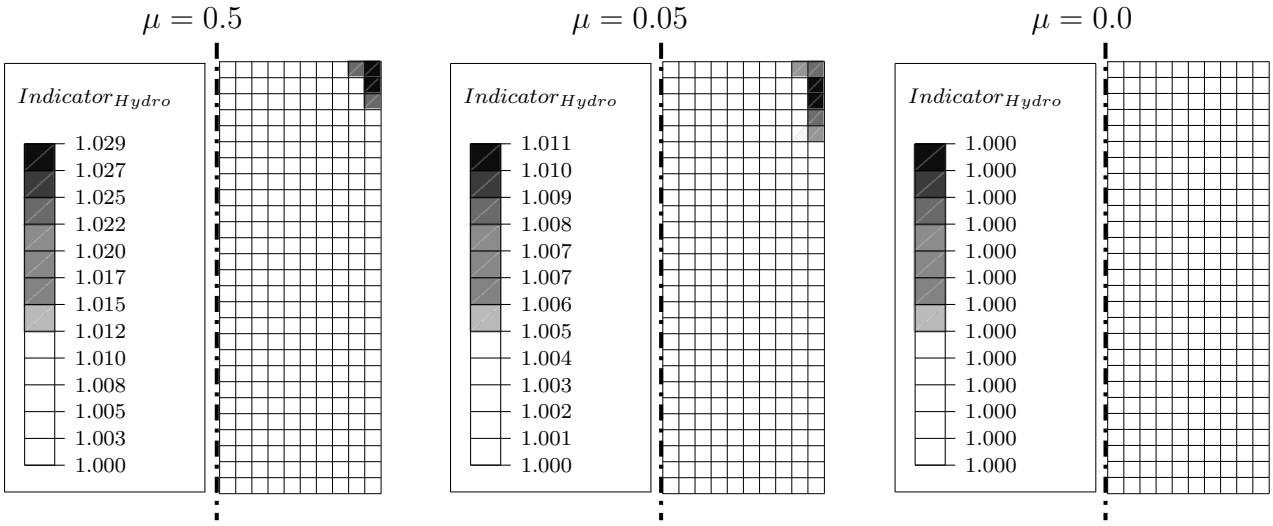

Figure 6: The $Indicator_{Hydro}$ mapped on the undeformed FE mesh with a varied friction coefficient.

In general it can be stated that the indicator is close to 1.0 for different friction coefficients and different regions in the rubber cylinder. The deviations to 1.0, especially for the highest friction coefficient of

0.5, do not result in a relevant amount of dissipation of energy within the MORPH based simulations (see figure 5). The maximum distortion, caused by friction to the contact lines, takes place in the area of the max($Indicator_{Hydro}$). The findings from the simulations support the statements from the analytical investigations (see section 3). It is shown that the behavior of the globally measured reaction force over the globally measured displacement is mainly driven by the hydrostatic load of the specimen. Non-hydrostatic contributions can be neglected in any further investigations.

5 Experimental Results and Evaluation

Figure 7 shows the force-displacement-curve of the cyclic hydrostatic compression test. A clear dependency on the loading path is observable. The investigated EPDM shows similar behavior like general rubbery materials in non-hydrostatic multi-hysteresis tests. The dissipated energy appears as a hysteresis loop in the force-displacement diagram. Additionally, material softening is observable. Due to the scattering within the force and displacement signals, the experimental data is smoothed via a combination of Savitzky-Golay filter (see Savitzky and Golay (1964)) and a moving average with respect to the displacement and the reaction force.

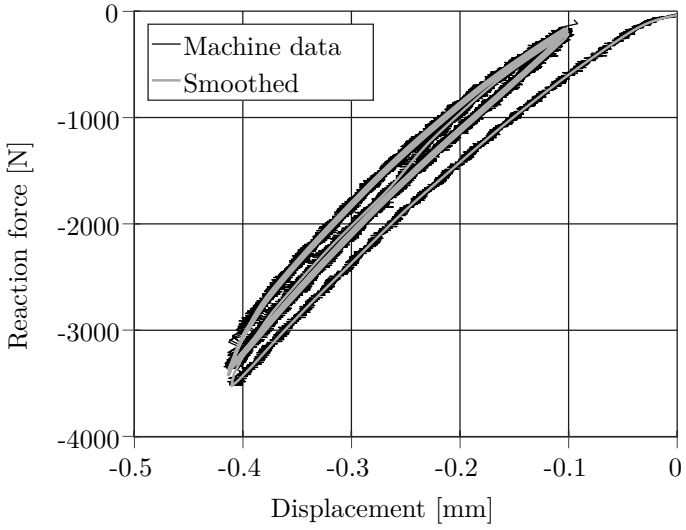

Figure 7: Cyclic volumetric compression test - Comparison of machine and smoothed data

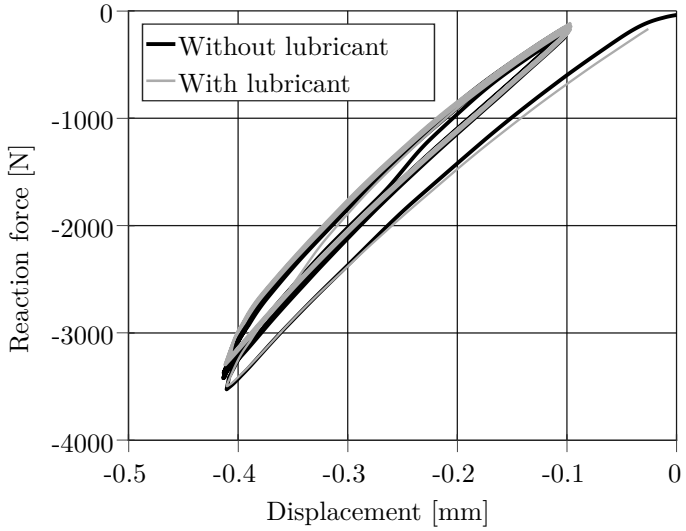

Figure 8: Comparison of resulting smoothed data with and without using soap as lubricant.

To investigate, if only the possible friction between the specimen and the surrounding fixture is responsible for the hysteresis loop, a second test with the use of a lubricant is conducted. The lubricant causes a decrease of the friction coefficient. A comparison of both tests, results in the conclusion that the dissipated energy due to friction is neglectable compared to the dissipated energy of the rubber material itself, see figure 8. The simulation behind figure 5 (see section 4) shows the same results regarding the influence of the friction coefficient on the global dissipated energy. The experimental compression modulus is derived by

$$K = \frac{\partial F_s}{\partial u} \cdot \frac{h}{A}. \tag{9}$$

Where u is the smoothed displacement signal, F_s is the smoothed force signal and h is the height of the specimen. Due to the smoothing the derived data near the turning points of the loading is ambiguous and not considered in the results shown in figure 9. However, the trends for the dependency of the compression modulus on load path and cyclic repetition are visible. For the first loading the compression modulus depends nearly linear on the applied pressure. This is less true for further stages of loading and unloading.

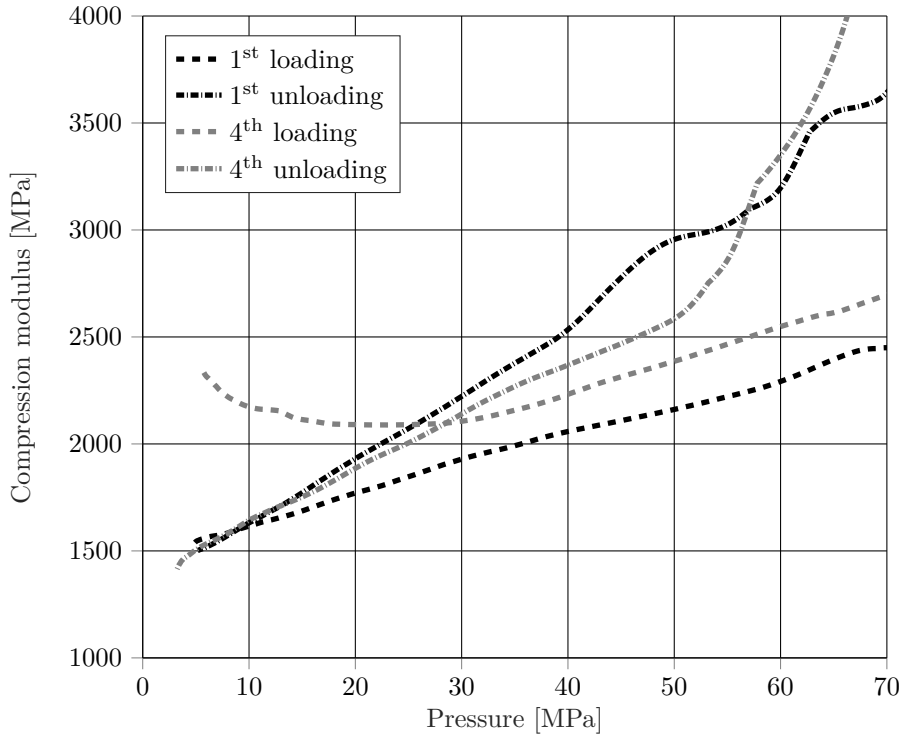

Figure 9: Comparison of the resulting compression modulus (experiment conducted with lubricant) for different stages of loading (cf. figure 1 (right)).

6 Conclusion and Outlook

Experimental investigations, focusing on the mechanical behavior of a rubber material under hydrostatic loading, are performed. For the investigations, a repeated loading of a cylindrical shaped specimen in a tight-fitting steel die is chosen. Furthermore, two different conditions are applied. These two conditions differ in terms of the friction coefficient between the specimen and the solid surrounding. The influence of the dissipated energy by friction is numerically and experimentally proven to be small in comparison with the dissipated energy by the rubber material. Analytical and numerical investigations are applied to reconstruct the experimental investigations. The analytical investigations demonstrate that the applied test procedure can be used to measure the material behavior under hydrostatic loading. The numerical investigations exhibits that an advanced material model, like MORPH, can describe the inelastic material behavior under non-hydrostatic loadings, but behaves like the Neo-Hooke model (by definition) under hydrostatic loadings. By evaluating the test results under hydrostatic loadings, the following can be extracted.

- The compression modulus is a function of the loading intensity and the loading history.
- The dependency of the loading history is significantly more distinct for the loading compared to the unloading.
- A general increase of the compression modulus with repeated loading is visible. For pressure levels, lower than 10 MPa this increase amounts to more than 55 %.
- The compression modulus is nearly independent on the loading history for the unloading case.
- A nearly steady material behavior is reached after the first loading cycle.

A possible explanation for the observed material behavior under hydrostatic loadings is shown in figure 10. Filled rubber contains inhomogeneities with different compression behavior. As an example, solid inhomogeneities (e.g. accumulated filler) or gaseous inhomogeneities (e.g. trapped air) are considered. The compression modulus of the solid inhomogeneities (e.g. carbon black particles) and the rubber matrix is serval magnitudes greater than the compression modulus of gaseous inhomogeneities. On a small scale, the globally applied small hydrostatic deformations can therefore lead to non-hydrostatic large deformations. As it is well known, strain energy is dissipated under these conditions.

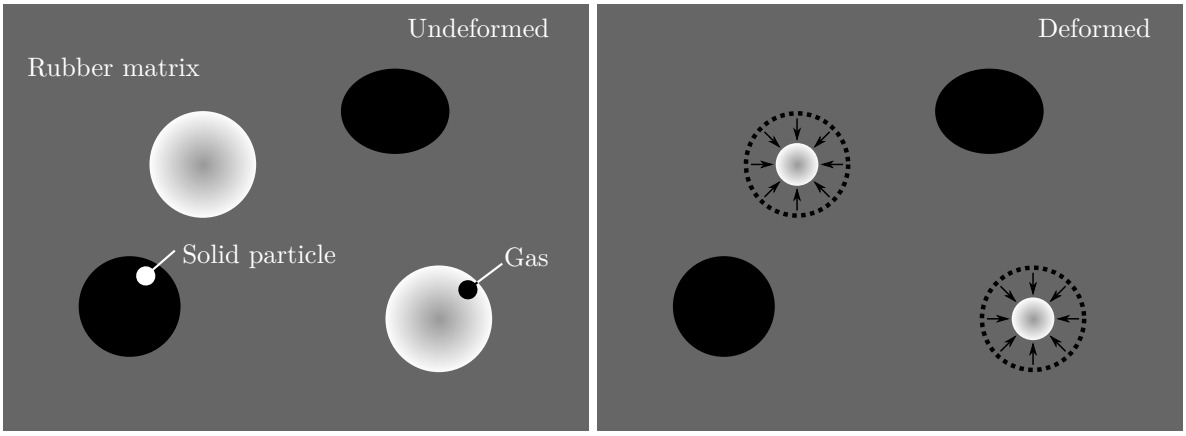

Figure 10: A possible explanation for the observed material behavior under hydrostatic loading.

Thus, working with a constant compression modulus is only a rough description of the reality for strong hydrostatic loadings. For these cases, a modeling of the compression modulus as a function of the loading intensity, loading history and loading/unloading distinction could lead to more realistic results in finite element applications. To verify these statements, additional investigations with a test device designed to be more sensitive to small deformations is advisable.

References

Besdo, D.; Ihlemann, J.: A phenomenological constitutive model for rubberlike materials and its numerical applications. *International Journal of Plasticity, 19, pp. 1019-1036*.

Horgan, C. O.; Murphy, J. G.: Compression tests and constitutive models for the slight compressibility of elastic rubber-like materials. *Int J Eng Sci 47 (2009), 1232-1239*.

Horgan, C. O.; Murphy, J. G.: A generalization of hencky's strain energy density to model the large deformations of slightly compressible rubbers. *Mechanics of Materials 41 (2009), 943-950*.

Horgan, C. O.; Murphy, J. G.: On the volumetric part of strain-energy functions used in the constitutive modeling of slightly compressible solid rubbers. *Int J Solids Struct 46 (2009), 3078-3085*.

Ilseng, A.; Skallerud, B. H.; Clausen, A. H.: Volumetric compression of hnbr and fkm elastomers. *Constitutive Models for Rubber IX (2015), 235-241*.

Juhre, D.; Ihlemann, J.; Alshuth, T.; Klauke, R.: Some remarks on influence of inelasticity on fatigue life of filled elastomers. *Plastics, rubber and composites. - London : Taylor and Francis, Bd. 40.2011, 4, pp. 180-184*.

Rajagopal, K. R.; Saccomandi, K. R.: The mechanics and mathematics of the effect of pressure on the shear modulus of elastomers. *Proc R Soc A 465 (2009), 3859-3874*.

Rivlin, R. S.; Saunders, D.: Large elastic deformations of isotropic materials. vii. experiments on the deformation of rubber. *Philosophical Transactions of the Royal Society of London A: Mathematical, Physical and Engineering Sciences, 243(865), 251-288*.

Savitzky, A.; Golay, M.: Smoothing and differentiation of data by simplified least squares procedures. *Analytical Chemistry. 36 (8), 1627-39*.

Treloar, L.: Stress-strain data for vulcanized rubber under various types of deformation. *Rubber Chemistry and Technology, 17(4), 813-825*.

Zienkiewicz, O.; Taylor, R.; Zhu, J.: *The Finite Element Method: Its Basis and Fundamentals* (2013).

Zimmermann, J.; Stommel, M.: The mechanical behaviour of rubber under hydrostatic compression and the effect on the results of finite element analyses. *Arch Appl Mech 83 (2013), 293-302*.

Address: Oliver Gehrmann, Nils Hendrik Kröger, Peter Erren
Deutsches Institut für Kautschuktechnologie e.V., Eupener Straße 33, 30519 Hanover, Germany
email: `Oliver.Gehrmann@DIKautschuk.de`

Address: Daniel Juhre, Institut für Mechanik, Otto-von-Guericke-Universitä Magdeburg
Universitätspaltz 2, D-39106 Magdeburg
email: `Daniel.Juhre@ovgu.de`